Reduction of the usable wind-work on the general circulation by forced symmetric instability

L. N. Thomas[1] and J. R. Taylor[2]

Received 13 July 2010; accepted 9 August 2010; published 30 September 2010.

[1] Winds aligned with geostrophic currents input energy into the ocean circulation. For baroclinic, surface-intensified currents, winds of this orientation (i.e., down-front winds) reduce the potential vorticity in the mixed layer, making the flow susceptible to symmetric instability (SI). SI is a submesoscale shear instability that draws its energy from baroclinic, geostrophic currents. High-resolution numerical simulations are used to demonstrate how forced SI driven by down-front winds extracts energy from the geostrophic flow at a rate proportional to the Ekman buoyancy flux, the dot product of the Ekman transport and the surface buoyancy gradient. The kinetic energy (KE) going into SI is converted to 3D turbulence through a secondary shear instability and ultimately dissipated at small scales. Thus under the conditions where winds input KE to the circulation, some of the KE of baroclinic currents is dissipated by this mechanism. The net result of this submesoscale sink of KE is to reduce the usable wind-work, i.e., the wind-induced rate of KE increase, by an amount that depends on the wind-stress and the change in geostrophic velocity across the mixed layer. **Citation:** Thomas, L. N., and J. R. Taylor (2010), Reduction of the usable wind-work on the general circulation by forced symmetric instability, *Geophys. Res. Lett.*, *37*, L18606, doi:10.1029/2010GL044680.

1. Introduction

[2] Aside from the tides, the main source of energy for the ocean circulation is the wind-work, $\boldsymbol{\tau}_w \cdot \mathbf{u}_g^s$, where $\boldsymbol{\tau}_w$ is the wind-stress and $\mathbf{u}_g^s$ is the geostrophic velocity at the sea surface [*Wunsch and Ferrari*, 2004]. Maps of $\boldsymbol{\tau}_w \cdot \mathbf{u}_g^s$ reveal that most of the energy input by the winds occurs at the Antarctic Circumpolar Current, the Kuroshio, and the Gulf Stream/North Atlantic current, all regions characterized by ocean fronts [*Wunsch*, 1998]. A fundamental question in the theory of the ocean circulation, a definitive answer to which is not known, is how and where this energy input by the winds is dissipated [*Ferrari and Wunsch*, 2009]. In this article we will present arguments that highlight frontal regions, where the wind-work is largest, as locations of enhanced dissipation. The arguments are based on the dynamics of the potential vorticity (PV), a tracer that controls the circulation and that is an indicator of flow stability [*Rhines*, 1986].

[3] The PV is changed by frictional and diabatic processes. Thus wind-induced friction acting on ocean fronts not only affects the energetics of the circulation but also modifies its potential vorticity (PV). In particular, when the winds are "down-front", that is, directed along the geostrophic shear, the PV is reduced in the surface boundary layer [*Thomas*, 2005]. Baroclinic surface currents with low PV are susceptible to a variety of submesoscale frontal instabilities that are fueled by the kinetic and potential energy of the currents [*Thomas et al.*, 2008]. These submesoscale instabilities have been implicated as mediators in the dissipation of the ocean circulation's energy as they can drive a forward cascade of energy from large to small scales [*Capet et al.*, 2008; *Molemaker et al.*, 2010]. One submesoscale instability that could be quite effective at removing energy from the circulation is symmetric instability.

[4] Symmetric instability (SI) develops in a geostrophic current when its Ertel PV, $q = (f\hat{k} + \nabla \times \mathbf{u}) \cdot \nabla b$ (where f is the Coriolis parameter, $\hat{k}$ is a unit vector in the vertical, $\mathbf{u}$ is the velocity, $b = -g\rho/\rho_o$ is the buoyancy, g is the acceleration due to gravity, ρ is the density, and ρ_o is a reference density), takes the opposite sign of f as a consequence of the vertical shear and horizontal density gradient of that current [*Hoskins*, 1974]. Frontal flows, with their strong baroclinicity, tend to have relatively low PV, and are hence preconditioned for SI. Atmospheric forcing that is associated with an extraction of PV from the ocean surface, such as cooling or down-front winds, can drive frontal flows symmetrically unstable, as has been observed at the subpolar front of the Japan/East Sea, the Gulf Stream, and Kuroshio [*Thomas and Lee*, 2005; *Joyce et al.*, 2009; E. D'Asaro et al., Enhanced mixing and energy dissipation at ocean fronts, submitted manuscript, 2010].

[5] SI is a shear instability that extracts kinetic energy (KE) from geostrophic flows [*Bennetts and Hoskins*, 1979] and thus could play a role in the dissipation of the ocean circulation's energy. It should be emphasized that SI is only a mediator of dissipation since its characteristic length scales are several orders of magnitude larger than those on which molecular viscosity can act. Turbulence on scales smaller than SI is thus required for the removal of energy by friction. Indeed, *Taylor and Ferrari* [2009] found that, in its finite amplitude, SI develops secondary instabilities which, in turn, cascade energy to small scales where molecular dissipation occurs. Identifying the steps involved in the transfer of energy from the geostrophic flow to dissipation via wind-forced SI and quantifying the rate at which this transfer occurs is the objective of this article.

2. Energetics of Wind-Forced Symmetric Instability

[6] The first step in assessing the role of SI in the dissipation of the ocean circulation is to characterize the processes responsible for the production of SI's kinetic energy.

[1]Department of Environmental Earth System Science, Stanford University, Stanford, California, USA.
[2]Department of Earth, Atmospheric, and Planetary Sciences, Massachusetts Institute of Technology, Cambridge, Massachusetts, USA.

0094-8276/10/2010GL044680

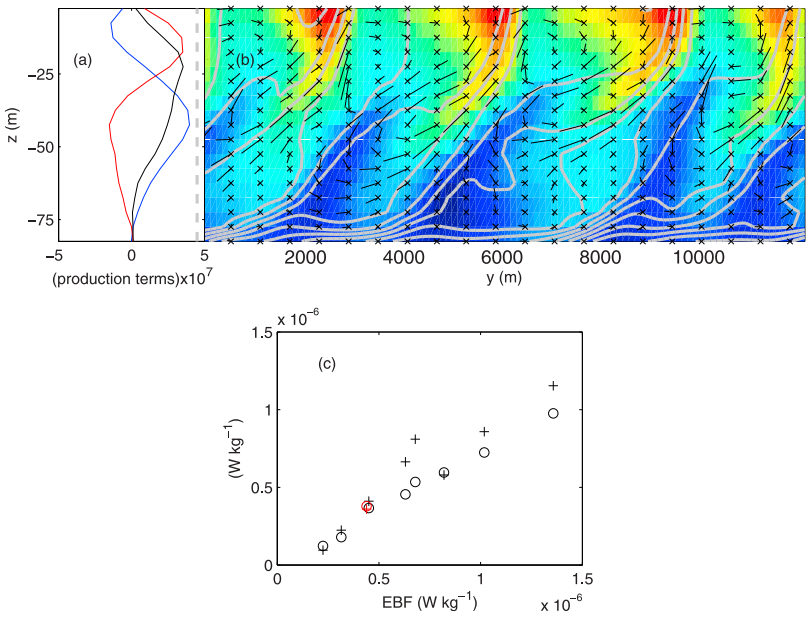

Figure 1. The structure of SI in a frontal zone with buoyancy gradient $S^2 = 6.3 \times 10^{-7}$ s^{-2} forced by a down-front wind-stress of strength 0.1 N m^{-2} and the KE production terms responsible for its growth. (a) The EBF (gray dashed) and profiles of $\overline{w'b'}$ (red), $\mathcal{P}$ (blue), and $\mathcal{P} + \overline{w'b'}$, (black), all quantities are in units of W kg^{-1}. (b) The secondary circulation (vectors, x's indicate vector tails), zonal velocity (shades), and density (gray contours). Warm (cool) shades indicate higher (lower) values of the zonal velocity. (c) Scatter plot of the maximum value with respect to z of the time-average of $\mathcal{P} + \overline{w'b'}$ (black circles) and $\mathcal{P}$ (black pluses) against the EBF for all of the ROMS frontal zone experiments. The same quantities evaluated using the LES solution are plotted in red.

To this end it is instructive to study SI in a simplified frontal system consisting of a zonal geostrophic flow $\overline{u}_g$ with a spatially uniform vertical shear and corresponding horizontal buoyancy gradient: $S^2 = -\partial\overline{b}/\partial y = f\partial\overline{u}_g/\partial z$ = constant. This two-dimensional "frontal zone" configuration has been used in previous numerical studies of forced SI and is ideal for examining the dependence of SI on the strength of the front and the forcing [*Thomas*, 2005; *Taylor and Ferrari*, 2009, 2010]. However, since $\partial\overline{b}/\partial y$ is constant, SI is not allowed to modify the strength of the front. As a result, a reservoir of available potential energy associated with the front is maintained. *Thomas* [2005] performed a series of numerical experiments using the hydrostatic ROMS model [*Shchepetkin and McWilliams*, 2005] to study the PV dynamics of SI forced by down-front winds. Output from these same simulations will be reanalyzed in terms of the energetics. Details of the flow, forcing, and numerical parameters are given by *Thomas* [2005].

[7] An example of the structure of the density and velocity fields associated with forced SI is shown in Figure 1b. The zonal velocity is shaped by the secondary circulation associated with SI. Fluid with low (high) zonal momentum is upwelled (downwelled), suggesting that there is a correlation between zonal and vertical velocities and therefore a Reynolds stress. This Reynolds stress can be quantified as $-\rho_o\overline{u'w'}$ (the overline denotes a y-average and the primes the deviation from that average). The Reynolds stress (not shown) peaks near the middle of the boundary layer at a value approaching the applied wind-stress of 0.1 N m^{-2}. SI thus drives a momentum flux that is down the mean gradient, homogenizing the geostrophic flow and lowering its average KE. The rate at which SI extracts energy from the geostrophic flow is the geostrophic shear production (GSP), $\mathcal{P} = -\overline{u'w'}S^2/f$, which is positive over much of the boundary layer (Figure 1a). In the more stratified portion of the boundary layer ($z < -25$ m), SI mixes density, as reflected by the negative buoyancy flux, $\overline{w'b'}$, it induces. Above this region a convective layer develops where the buoyancy flux is positive, similar to what was found in the large eddy simulations (LES) of forced SI of *Taylor and Ferrari* [2010]. Thus both the GSP and the buoyancy flux can act as sources of KE. In a quasi-steady state, $\mathcal{P} + \overline{w'b'}$, when integrated over the boundary layer depth, must be balanced by dissipation. Thus to quantify the dissipation associated with SI, $\mathcal{P} + \overline{w'b'}$ and its dependence on the frontal and forcing parameters should be determined. We use theory and numerical simulations to perform this calculation.

[8] Following *Taylor and Ferrari* [2010], momentum and buoyancy budgets for the spatially-averaged fields can be used to construct a relation between $\mathcal{P} + \overline{w'b'}$ and the forcing and frontal parameters. Within the boundary layer, the Coriolis force is balanced by the convergence of advective and viscous momentum fluxes, as in a turbulent Ekman layer, i.e.,

$$-f\overline{v} + \frac{\partial}{\partial z}\overline{u'w'} = \frac{1}{\rho_o}\frac{\partial\overline{\tau}^x}{\partial z}, \tag{1}$$

where τ^x is the zonal frictional stress. The spatially-averaged buoyancy field evolves with time following the equation:

$$\frac{\partial\overline{b}}{\partial t} - S^2\overline{v} + \frac{\partial}{\partial z}\overline{w'b'} = -\frac{\partial\overline{F}_b}{\partial z} \tag{2}$$

where F_b is a non-advective, diffusive buoyancy flux. Multiplying (1) by S^2/f, integrating the equation in the ver-

tical and then subtracting the result from the vertical integral of (2) yields the following expression

$$\mathcal{P} + \overline{w'b'} = \mathrm{EBF} + \overline{F}_b^{atm} + \int_z^0 \frac{\partial \overline{b}}{\partial t} dz \tag{3}$$

where F_b^{atm} is the buoyancy flux from the ocean to the atmosphere and

$$\mathrm{EBF} = \frac{\overline{\tau}_w^x}{\rho_o f} S^2 \tag{4}$$

is the Ekman buoyancy flux (also known as the wind-driven buoyancy flux [e.g., *Thomas*, 2005]) which reflects the tendency for the Ekman flow to destabilize the water column when the wind-stress, τ_w^x, is down-front [*Thomas and Lee*, 2005]. Note that for a vector wind field, EBF = $\mathbf{M}_e \cdot \nabla_h b$, where $\mathbf{M}_e = \boldsymbol{\tau}_w \times \mathbf{f}/(\rho_o f^2)$ is the Ekman transport and $\nabla_h b$ is the surface buoyancy gradient. The terms involving the molecular viscosity and diffusivity in (3) have been neglected since they are most important in a viscous/diffusive sublayer near $z = 0$ which is not the focus of this study. In the absence of a surface buoyancy flux ($\overline{F}_b^{atm} = 0$) the equation predicts that the EBF sets the strength of $\mathcal{P} + \overline{w'b'}$. It can be shown that the last term in (3) only controls the vertical structure of $\mathcal{P} + \overline{w'b'}$ and not its magnitude. When $\partial\overline{b}/\partial t$ is constant in the boundary layer, $\mathcal{P} + \overline{w'b'}$ is a linear function of z [*Taylor and Ferrari*, 2010].

[9] The theoretical prediction (3) can be tested using the numerical experiments of *Thomas* [2005] which cover a wide range of EBF values. To this end, the shear production and buoyancy flux averaged over the last two inertial periods of each experiment were calculated and their maximum value with respect to z was compared to the EBF (Figure 1c). The comparison confirms that the EBF controls the strength of the GSP and $\mathcal{P} + \overline{w'b'}$.

3. Turbulent Dissipation of Wind-Forced SI

[10] The energy extracted from a front by SI must be ultimately dissipated. What are the processes responsible for this dissipation? The simulations described above cannot address what processes are responsible for the dissipation because they parameterize rather than resolve small scale turbulence. In order to address this question, we have conducted a 3D large eddy simulation (LES) with parameters chosen to match those used in the experiment shown in Figure 1b. The LES code solves the non-hydrostatic, incompressible, Boussinesq primitive equations and uses a pseudo-spectral method in the two periodic horizontal directions and second-order finite differences in the vertical. A horizontal resolution of 5.8m has been used, while the grid is nonuniform in the vertical with a spacing of 0.32m at the top of the domain and 1.64m at the bottom. Following *Taylor and Ferrari* [2010], a modified constant Smagorinsky subgrid-scale model with a turbulent Prandtl number of one has been employed. The LES does not capture or include a parameterization for the dynamics or energetics of surface gravity waves. Details of the numerical method and model configuration are given by *Taylor* [2008] and *Bewley* [2010] and in the auxiliary material.[1]

[11] A visualization of the density and velocity field from the LES is shown in Figure 2a, with along-front velocity shown in color shading, cross-front and vertical velocity shown using arrows, and three isopycnal surfaces contoured in white. Along-isopycnal flow indicative of SI can be seen at mid-depths, carrying high momentum fluid downwards. The vertical exchange of along-front momentum associated with SI and smaller scale motions results in a negative $\overline{u'w'}$, and therefore a positive GSP. The main sources and sinks in the turbulent kinetic energy budget are shown in Figure 2b. $\mathcal{P} + \overline{w'b'}$ is dominated by the GSP to a much greater degree in the LES than in the 2D simulations, indicating that the turbulence gets its energy almost exclusively from the geostrophic flow. Similar to the 2D simulations, the GSP peaks at a value close to the EBF and decays nearly linearly with depth. The correspondence between the EBF and $\mathcal{P} + \overline{w'b'}$ in the fully 3D LES agrees with that found in the ROMS experiments (e.g., Figure 1c), validating the scaling.

[12] The buoyancy flux is negative over much of the boundary layer, except in a convective layer for $z > -13.4$m. *Taylor and Ferrari* [2010] observed similar convective layers forming in their simulations forced by surface heat loss and derived a scaling for their thickness h, which given the parameters of the wind-forced experiment yields h = 13 m, consistent with the model results. Note that unlike the simulations of *Taylor and Ferrari* [2010], the GSP and forced SI extend well into the convective layer in the wind-driven LES reported here. As described in the auxiliary material, shear production associated with ageostrophic shear is large near the surface, reflecting wind-driven Ekman layer turbulence. However, when integrated over the boundary layer, the amount of turbulence generated by the GSP at the expense of the thermal wind is about twice as large as the turbulence produced directly by the wind-stress. The dissipation that cannot be attributed to Ekman turbulence, ϵ_{SI}, (the solid curve in Figure 2a) mirrors $\mathcal{P} + \overline{w'b'}$, with the exception of a thin layer near the surface where the vertical transport terms play a leading role. The balance between ϵ_{SI} and $\mathcal{P} + \overline{w'b'}$ illustrates how the kinetic energy removed from the geostrophic flow ultimately leaves the system either through friction or diapycnal mixing. The way in which this occurs in Fourier space is explored below.

[13] To identify the scales associated with energy production and transfer, it is useful to consider the kinetic energy equation in Fourier space:

$$\frac{\partial}{\partial t}\Re[\hat{\mathbf{u}}^* \cdot \hat{\mathbf{u}}] = \Re\left[\underbrace{-\hat{\mathbf{u}}^* \cdot \mathbf{u} \cdot \widehat{\nabla}\mathbf{u}}_{ADV} \underbrace{-\hat{u}^* \hat{w} S^2/f}_{GSP} \underbrace{-\hat{\mathbf{u}}^* \cdot \widehat{\nabla p}/\rho_o}_{PRES} + \underbrace{\hat{w}^* \hat{b}}_{BFLUX} + \underbrace{\hat{\mathbf{u}}^* \cdot \hat{\mathbf{F}}}_{FRIC}\right], \tag{5}$$

where the caret denotes a horizontal Fourier transform, p is the pressure, and $\mathbf{F}$ represents the combined molecular and modeled subgrid-scale frictional forces. The spectral energy flux at each cross-front wavenumber, Π (k_y), can be calculated by taking the cumulative integral, or ogive, of the advection term in equation (5)

$$\Pi(k_y, z, t) = \int \int_{k_y}^{k_y^{\max}} ADV dk_y' dk_x, \tag{6}$$

[1] Auxiliary materials are available in the HTML. doi:10.1029/2010GL044680.

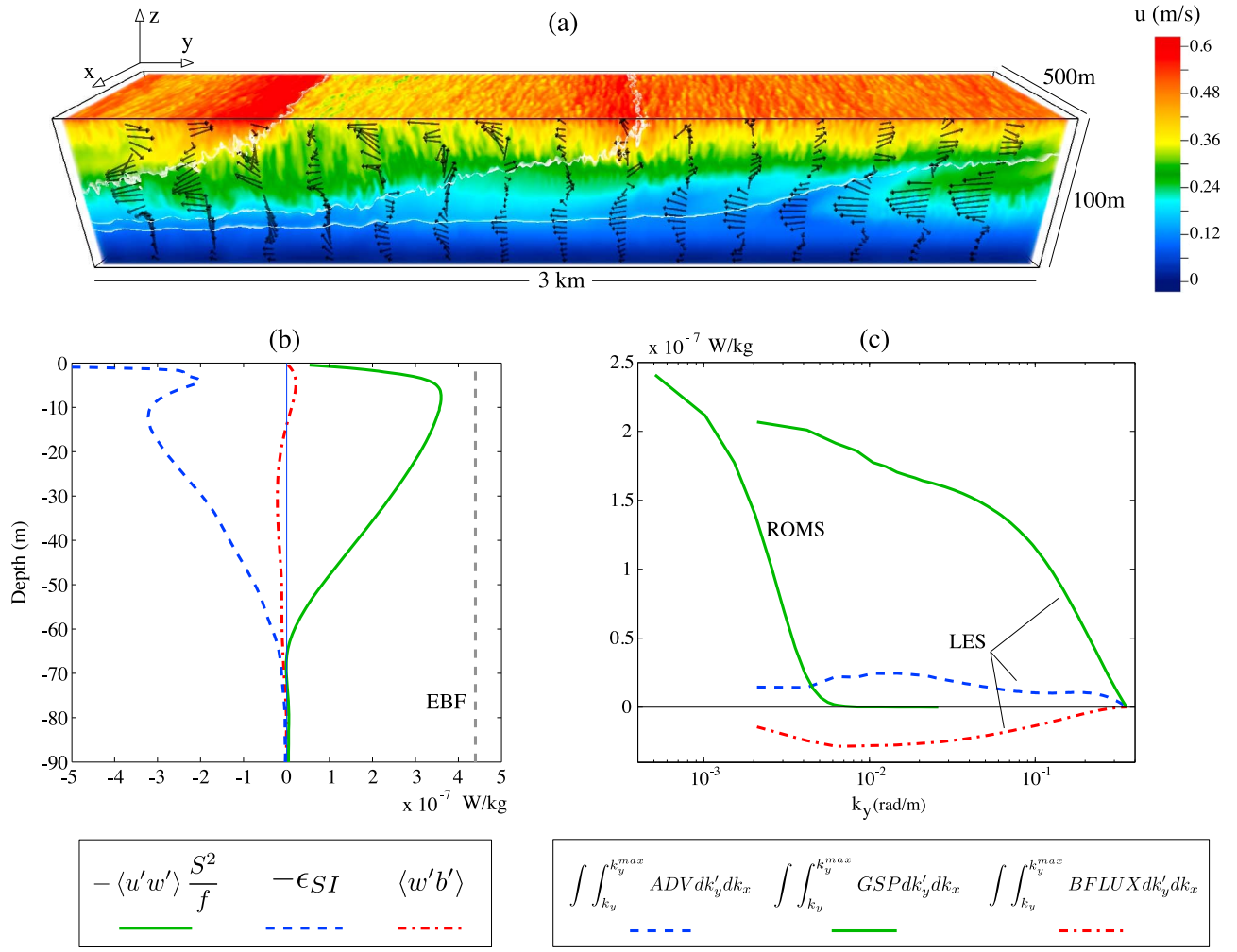

Figure 2. (a) A visualization of the buoyancy and velocity field in the LES. Color shading shows the along-front velocity, u. The velocity field in the $y-z$ plane is shown using arrows, and three isopycnal surfaces are shown in white. The vertical coordinate and velocity vectors have been exaggerated by a factor of 5. (b) Terms in the mean TKE budget for the LES. The average operator, $\langle\cdot\rangle$, is applied over horizontal planes and for two inertial periods. (c) Cumulative spectral integral, or ogive, for the advection, GSP, and buoyancy flux terms as a function of cross-front wavenumber. Each term has been averaged from $-60 < z < -13.4$m over a time window of two inertial periods. The integrated GSP for the ROMS simulation is also shown for comparison.

where $k_y^{\max}$ is the maximum discrete wavenumber used in the simulations. When $\Pi > 0$, energy is transferred forward in spectral space from large to small scales. It is also useful to consider the ogives of the GSP and buoyancy flux terms. When evaluated at $k_y = 0$, the ogives return the mean GSP and buoyancy flux as shown in Figure 2b. For $k_y \neq 0$, the ogives show the cumulative contribution to the GSP and buoyancy flux for scales with cross-front wavenumber larger than k_y. The ogives of the advection, GSP, and buoyancy flux terms are shown in Figure 2c. In order to focus on the SI region and exclude the convective layer, the ogives in Figure 2c have been averaged over the interval $-60\text{m} < z < -13.4\text{m}$. The sign of Π (k_y) implies that energy is transferred down-scale for all wavenumbers in the LES, and the largest down-scale energy flux is associated with the transfer out of the SI modes. The individual wavenumber contributions to the GSP are largest for $k_y < 10^{-2}$ rad/m (not shown), but as seen in the ogive in Figure 2c, small scales make a very significant cumulative contribution to the GSP in the LES. For comparison, the GSP ogive from the ROMS simulation is also shown. Although the mean GSP is similar in the LES and ROMS, the ROMS simulation does not capture the contribution to the GSP from the small scales.

4. Discussion

[14] We have shown that KE is preferentially dissipated at fronts forced by down-front winds due to the formation of SI and its secondary instabilities. These same winds also input KE to the circulation via the wind-work. This implies that the rate of KE increase by wind forcing is reduced relative to the wind-work because of the KE sink associated with SI and small-scale shear instabilities. To determine the parameter dependence of this reduction, the net dissipation associated with SI, $\int \rho_o \epsilon_{SI} dz$, was calculated. As shown in Figure 2b, ϵ_{SI} counteracts the geostrophic shear production, which peaks near the surface at a value approaching the EBF and follows a near-linear profile with depth in the surface

boundary layer, i.e., $\epsilon_{SI} \approx \mathcal{P} \approx \mathrm{EBF}(z/\overline{H} + 1)$, where $\overline{H}$ is the depth of the surface boundary layer averaged in y. Given this profile, $\int \rho_o \epsilon_{SI} dz \approx \overline{H}\,(\mathrm{EBF})/2 = \overline{\tau}^x_w \overline{\Delta u_g}/2$ where $\overline{\Delta u_g} = S^2\overline{H}/f$ is the change in geostrophic velocity across the surface boundary layer. It therefore follows that the amount of wind-work that is available for increasing the KE of the circulation, what we will refer to as the *usable wind-work*, is

$$\text{Usable wind} - \text{work} = \begin{cases} \overline{\boldsymbol{\tau}_w} \cdot \left(\overline{\mathbf{u}^s_g} - \frac{1}{2}\overline{\Delta \mathbf{u}_g} \right), & \overline{\boldsymbol{\tau}_w} \cdot \overline{\Delta \mathbf{u}_g} > 0 \\ \overline{\boldsymbol{\tau}_w} \cdot \overline{\mathbf{u}^s_g}, & \overline{\boldsymbol{\tau}_w} \cdot \overline{\Delta \mathbf{u}_g} < 0 \end{cases}, \tag{7}$$

where the result has been generalized for a vector wind-field and the overline represents a spatial average over the lateral scales associated with SI. The usable wind-work is reduced when the winds are down-front ($\overline{\boldsymbol{\tau}_w} \cdot \overline{\Delta \mathbf{u}_g} > 0$) and is unaffected by up-front winds which restratify the surface boundary layer and hence suppress rather than fuel SI [*Thomas and Ferrari*, 2008]. Thus the fractional reduction of the usable wind-work relative to $\overline{\boldsymbol{\tau}_w} \cdot \overline{\mathbf{u}^s_g}$ depends on the ratio of the change in geostrophic velocity across the mixed layer to the value of the geostrophic flow at the surface.

5. Conclusions

[15] Scaling arguments, (3), and high-resolution numerical simulations predict that the dissipation of KE should be enhanced at fronts forced by down-front winds. D'Asaro et al. (submitted manuscript, 2010) describe observations of enhanced turbulence at a particularly sharp wind-forced front in the Kuroshio that support this prediction. The peak in the estimated dissipation that they observed coincided with the maximum in EBF and with negative PV, both indications that the elevated turbulence at the front may be at least partially attributable to wind-forced SI.

[16] The net effect of wind-forced SI is to reduce the usable wind-work (7). Evaluating its impact on the global energetics of the ocean would require integrating (7) over the area of the worlds oceans. D'Asaro et al. (submitted manuscript, 2010) made a first attempt at this calculation using output from the ECCO ocean state estimate [*Wunsch et al.*, 2009]. They estimated that dissipation at fronts leads to a reduction in the total usable wind-work of over 5% (i.e., resulting in > 0.05 TW of dissipation in the mixed layer). This is much smaller than the ~19 TW of dissipation associated with wind-driven ageostrophic motions, such as surface gravity waves, Ekman flow, etc. [e.g., *Wunsch and Ferrari*, 2004] but unlike this sink of wind-energy, dissipation associated with SI represents a loss of energy for the geostrophic circulation. The 5% reduction is likely an underestimate owing to the coarse resolution of the ECCO solution that cannot capture eddies. The presence of baroclinic eddies should only augment the net dissipation associated with wind-forced SI as surface density gradients and hence regions of positive EBF span a larger area in an eddy-filled ocean than in an eddy-free one. Estimating the significance of wind-forced SI in baroclinic eddies on the energetics of the ocean circulation will be the subject of future research.

[17] **Acknowledgments.** L.T. was supported by the NSF grant OCE-0549699 and the Office of Naval Research grant N00014-09-1-0202. J.R.T was supported by a Mathematical Sciences Postdoctoral Research Fellowship (MSPRF). We credit Eric D'Asaro for coming up with the term Ekman buoyancy flux (EBF) which more accurately describes destratification by Ekman advection of buoyancy.

References

Bennetts, D. A., and B. J. Hoskins (1979), Conditional symmetric instability—A possible explanation for frontal rainbands, *Q. J. R. Meteorol. Soc.*, *105*, 945–962.

Bewley, T. (2010), *Numerical Renaissance: Simulation, Optimization, and Control*, Renaissance, San Diego, Calif. (Available at http://numerical-renaissance.com)

Capet, X., J. C. McWilliams, M. J. Molemaker, and A. F. Shchepetkin (2008), Mesoscale to submesoscale transition in the California Current system: Energy balance and flux, *J. Phys. Oceanogr.*, *38*, 2256–2269.

Ferrari, R., and C. Wunsch (2009), Ocean circulation kinetic energy: Reservoirs, sources, and sinks, *Annu. Rev. Fluid Mech.*, *41*, 253–282.

Hoskins, B. J. (1974), The role of potential vorticity in symmetric stability and instability, *Q. J. R. Meteorol. Soc.*, *100*, 480–482.

Joyce, T. M., L. N. Thomas, and F. Bahr (2009), Wintertime observations of Subtropical Mode Water formation within the Gulf Stream, *Geophys. Res. Lett.*, *36*, L02607, doi:10.1029/2008GL035918.

Molemaker, J., J. C. McWilliams, and X. Capet (2010), Balanced and unbalanced routes to dissipation in an equilibrated Eady flow, *J. Fluid Mech.*, *654*, 35–63.

Rhines, P. B. (1986), Vorticity dynamics of the oceanic general circulation, *Annu. Rev. Fluid Mech.*, *18*, 433–497.

Shchepetkin, A. F., and J. C. McWilliams (2005), The Regional Ocean Modeling System (ROMS): A split-explicit, free-surface, topography-following coordinate oceanic model, *Ocean Modell.*, *9*, 347–404.

Taylor, J. (2008), Numerical simulations of the stratified oceanic bottom boundary layer, Ph.D. thesis, Univ. of Calif., San Diego.

Taylor, J., and R. Ferrari (2009), The role of secondary shear instabilities in the equilibration of symmetric instability, *J. Fluid Mech.*, *622*, 103–113.

Taylor, J., and R. Ferrari (2010), Turbulent convection at a mixed-layer front, *J. Phys. Oceanogr.*, in press.

Thomas, L. N. (2005), Destruction of potential vorticity by winds, *J. Phys. Oceanogr.*, *35*, 2457–2466.

Thomas, L. N., and R. Ferrari (2008), Friction, frontogenesis, and the stratification of the surface mixed layer, *J. Phys. Oceanogr.*, *38*, 2501–2518.

Thomas, L. N., and C. M. Lee (2005), Intensification of ocean fronts by down-front winds, *J. Phys. Oceanogr.*, *35*, 1086–1102.

Thomas, L., A. Tandon, and A. Mahadevan (2008), Submesoscale processes and dynamics, in *Eddy-Resolving Ocean Modeling*, *Geophys. Monogr. Ser.*, vol. 177, edited by M. Hecht and H. Hasumi, pp. 17–38, AGU, Washington, D. C.

Wunsch, C. (1998), The work done by the wind on the oceanic general circulation, *J. Phys. Oceanogr.*, *28*, 2332–2340.

Wunsch, C., and R. Ferrari (2004), Vertical mixing, energy, and the general circulation of the oceans, *Annu. Rev. Fluid Mech.*, *36*, 281–314.

Wunsch, C., P. Heimbach, R. Ponte, and I. Fukumori (2009), The global general circulation of the ocean estimated by the ECCO-consortium, *Oceanography*, *22*, 88–103.

J. R. Taylor, Department of Earth, Atmospheric, and Planetary Sciences, Massachusetts Institute of Technology, 77 Massachusetts Ave., Cambridge, MA 02139-4307, USA.

L. N. Thomas, Department of Environmental Earth System Science, Stanford University, 473 Via Ortega, Y2E2 Bldg., Stanford, CA 94305-4215, USA. (leift@stanford.edu)